

A lattice study of a chirally invariant Higgs-Yukawa model including a higher dimensional Φ^6 -term

David Y.-J. Chu^a, Karl Jansen^b, Bastian Knippschild^c, C.-J. David Lin^d, Attila Nagy^{b,e}

^a*Department of Electrophysics, National Chiao-Tung University, Hsinchu 30010, Taiwan*

^b*NIC, DESY, Platanenallee 6, D-15738 Zeuthen, Germany*

^c*HISKP, Nussallee 14-16, D-53115 Bonn, Germany*

^d*Institute of Physics, National Chiao-Tung University, Hsinchu 30010, Taiwan*

^e*Humboldt-Universität zu Berlin, Institut für Physik, Newtonstr. 15, D-12489 Berlin, Germany*

Abstract

We discuss the non-thermal phase structure of a chirally invariant Higgs-Yukawa model on the lattice in the presence of a higher dimensional Φ^6 -term. For the exploration of the phase diagram we use analytical, lattice perturbative calculations of the constraint effective potential as well as numerical simulations. We also present first results of the effects of the Φ^6 -term on the lower Higgs boson mass bounds.

Keywords: lattice, Higgs-Yukawa model, vacuum stability,

1. Introduction

In this letter we investigate the influence of the addition of a dimension-6 operator to a chirally invariant Higgs-Yukawa model. This model can be understood as a limit of the standard model (SM) without gauge fields. In particular, we consider a complex scalar doublet and one doublet of mass-degenerate quarks. Our aim is to explore, whether a dimension-6 operator, for which we will employ a $(\varphi^\dagger\varphi)^3$ -term with a coupling constant λ_6 , can modify the phase structure of the Higgs-Yukawa sector of the SM and may alter the lower Higgs boson mass bound as already observed in [1, 2]. For a phenomenological analysis of a $(\varphi^\dagger\varphi)^3$ -term see e.g. [3, 4].

The motivation for adding a $(\varphi^\dagger\varphi)^3$ -term is twofold. First, since the Higgs-Yukawa sector of the SM is trivial, the cut-off cannot be removed and hence such a term is in principle allowed. In addition, if small values of the cut-off of $O(1) - O(10)\text{TeV}$ are considered as done in this work, such a term can have a significant effect. Second, the appearance of a $(\varphi^\dagger\varphi)^3$ -term can be understood to arise from an extension of the SM. Studying the system with such a term could hence provide bounds on the couplings of such extensions in case the lower Higgs boson mass bound is incompatible with the Higgs boson mass of about 126GeV . The effects of higher dimensional operators on the vacuum stability is discussed in [5, 6, 7].

We use a lattice regularization of the Higgs-Yukawa model which eventually also allows non-perturbative numerical simulations for large values of λ_6 . The notion of an exact lattice chiral symmetry [8] which derives from the Ginsparg-Wilson relation [9] allows us to emulate the continuum Higgs-Yukawa sector of the standard model on a discrete Euclidean space-time lattice. To this end, the overlap operator [10, 11] as a local [12] lattice Dirac operator has been employed to study the phase structure of the lattice theory [13, 14], to derive lower and upper Higgs boson mass bounds [15, 16, 17, 18] and to analyze the Higgs boson resonance non-perturbatively [19]. For a review, see [20].

For our investigations we perform analytical calculations of the phase structure of the model by computing the constraint effective potential (CEP) [21] to the first non-trivial order in lattice perturbation theory. In this calculation, we employ the same chirally invariant lattice formulation of the Higgs-Yukawa model as it is used for the numerical computations. We compare results for the phase structure obtained from numerical simulations to our perturbative predictions. In addition, we will provide first results for the lower Higgs boson mass bounds in the presence of the dimension-6 operator as obtained from the analytical, perturbative calculations of the CEP.

2. Basic definitions

In this work, we restrict ourselves to the case of one fermion doublet $\psi = (t, b)^T$ with mass degenerate quarks. The scalar fields are a complex doublet φ . Here, we will only provide the basic definitions of the model and refer to ref. [20] for a more

detailed explanation. In Euclidean space time the continuum action is given by:

$$S^{\text{cont}}[\bar{\psi}, \psi, \varphi] = \int d^4x \left\{ \frac{1}{2} (\partial_\mu \varphi)^\dagger (\partial^\mu \varphi) + \frac{1}{2} m_0^2 \varphi^\dagger \varphi + \lambda (\varphi^\dagger \varphi)^2 + \lambda_6 (\varphi^\dagger \varphi)^3 \right\} \\ + \int d^4x \{ \bar{t} \not{\partial} t + \bar{b} \not{\partial} b + y (\bar{\psi}_L \varphi b_R + \bar{\psi}_L \tilde{\varphi} t_R) + h.c. \}, \quad (1)$$

with $\tilde{\varphi} = i\tau_2 \varphi^*$ and τ_2 being the second Pauli matrix. Besides the standard bare parameters m_0^2 and λ for the Higgs potential and y for the Yukawa coupling, we add the dimension-6 operator $\lambda_6 (\varphi^\dagger \varphi)^3$ to the action.

For the numerical implementation of this model we use a polynomial hybrid Monte Carlo algorithm[22] with dynamical overlap fermions, see ref. [23] for details. On the lattice, it is convenient to rewrite the bosonic part of the action in the following way¹:

$$S_B[\Phi] = -\kappa \sum_{x,\mu} \Phi_x^\dagger [\Phi_{x+\mu} + \Phi_{x-\mu}] + \sum_x \left(\Phi_x^\dagger \Phi_x + \hat{\lambda} [\Phi_x^\dagger \Phi_x - 1]^2 + \hat{\lambda}_6 [\Phi_x^\dagger \Phi_x]^3 \right). \quad (2)$$

Here the scalar field, Φ , is represented as a real four-vector and the relation to the continuum notation is given by:

$$\varphi = \sqrt{2\kappa} \begin{pmatrix} \Phi^2 + i\Phi^1 \\ \Phi^0 - i\Phi^3 \end{pmatrix}, \quad m_0^2 = \frac{1 - 2\hat{\lambda} - 8\kappa}{\kappa}, \quad \lambda = \frac{\hat{\lambda}}{4\kappa^2}, \quad \lambda_6 = \frac{\hat{\lambda}_6}{8\kappa^3}. \quad (3)$$

As said above, our main goal is the exploration of the phase structure of the model in the presence of the $[\Phi_x^\dagger \Phi_x]^3$ term with coupling strength λ_6 . We will use the magnetization m as the order parameter². The magnetization is given by the modulus of the average scalar field and is related to the vacuum expectation value (*vev*) via:

$$m = \left\langle \left| \frac{1}{V} \sum_x \Phi_x \right| \right\rangle, \quad vev = \sqrt{2\kappa} \cdot m. \quad (4)$$

For a determination and detailed discussion of the phase structure of the model for $\lambda_6 = 0$, we refer to refs. [13, 14].

3. The constraint effective potential

Before resorting to numerical simulations, we study the phase structure analytically in lattice perturbation theory for which we employ the CEP [24, 21]. We assume the scalar field to be in the broken phase, so the scalar field decomposes into the Higgs mode, h , and the three Goldstone modes, g^α , with $\alpha = 1, 2, 3$. The

¹The lattice spacing is set to one throughout this paper.

²Here we are only interested in transitions between the symmetric and the spontaneously broken phases and thus will not consider the staggered magnetization [13, 14].

CEP $U(\hat{v})$ is described by the zero mode of the Higgs field, $\tilde{h}_0 = V^{-1/2}\hat{v}$. The perturbative calculations are done by keeping the lattice regularization explicitly, i.e. the overlap operator is used for the fermionic contribution and all sums over lattice momenta are performed numerically.

To obtain the potential the bosonic non-zero modes are integrated out. To do so, the bosonic action is separated into a Gaussian contribution which can be integrated out leading to the bosonic propagators. The remaining terms are treated as an interaction part and can be expanded in powers of the couplings. This separation into a Gaussian and an interaction part however is not unique and we employ two versions of the CEP.

A derivation of such a lattice constrained effective potential can be found in [14, 23]. Following the procedure in these references, the Gaussian contribution to the action reads:

$$S_1^{\text{gauss}}[h, g^\alpha] = \frac{1}{2} \sum_{p \neq 0} \left(\tilde{h}_{-p} (\hat{p}^2 + m_0^2) h_p + \sum_{\alpha} \tilde{g}_{-p}^{\alpha} (\hat{p}^2 + m_0^2) \tilde{g}_p^{\alpha} \right), \quad (5)$$

which leads to the propagator sums:

$$P_H = P_G = \frac{1}{V} \sum_{p \neq 0} \frac{1}{\hat{p}^2 + m_0^2}. \quad (6)$$

As in [15], m_0^2 is replaced by the renormalized masses in the propagator sums. The mass of the Goldstone boson is set explicitly to zero. This leads to:

$$P_H = \frac{1}{V} \sum_{p \neq 0} \frac{1}{\hat{p}^2 + m_H^2}, \quad P_G = \frac{1}{V} \sum_{p \neq 0} \frac{1}{\hat{p}^2}. \quad (7)$$

The determinant from integrating out eq. (5) is independent of \hat{v} and can therefore be neglected for the CEP.

The CEP up to the first order in λ and λ_6 is then given by:

$$U_1(\hat{v}) = U_f(\hat{v}) + \frac{m_0^2}{2} \hat{v}^2 + \lambda \hat{v}^4 + \lambda_6 \hat{v}^6 \\ + \lambda \cdot \hat{v}^2 \cdot 6(P_H + P_G) + \lambda_6 \cdot (\hat{v}^2 \cdot (45P_H^2 + 54P_G P_H + 45P_G^2) + \hat{v}^4 \cdot (15P_H + 9P_G)). \quad (8)$$

The fermionic contribution, U_f , originates from integrating out the fermions in the background of a constant field. It takes the form,

$$U_f(\hat{v}) = -\frac{4}{V} \sum_p \log \left| \nu^+(p) + y \cdot \hat{v} \cdot \left(1 - \frac{\nu^+(p)}{2\rho} \right) \right|^2, \quad (9)$$

where $\nu^\pm(p)$ denotes the eigenvalues of the overlap operator,

$$\nu^\pm(p) = \rho \left(1 + \frac{\pm i \sqrt{\tilde{p}^2 + r\hat{p}^2 - \rho}}{\sqrt{\tilde{p}^2 + (r\hat{p}^2 - \rho)^2}} \right), \quad \hat{p}^2 = 4 \sum_{\mu} \sin^2 \left(\frac{p_{\mu}}{2} \right), \quad \tilde{p}^2 = \sum_{\mu} \sin^2(p_{\mu}). \quad (10)$$

In this equation r denotes the Wilson parameter and ρ ($0 \leq \rho \leq 2r$) is a free parameter of the overlap operator which can be tuned to optimize its locality properties [12]. Throughout this work, we set $r = 1$ and $\rho = 1$.

In addition to the procedure leading to $U_1(\hat{v})$, eq. (8), another ansatz in performing the Gaussian integral is to collect all the terms that are quadratic in the bosonic non-zero modes from the self interaction:

$$S_2^{\text{gauss}}[h, g^\alpha] = \frac{1}{2} \sum_{p \neq 0} \left(\tilde{h}_{-p} (\hat{p}^2 + m_0^2 + 12\lambda\hat{v}^2 + 30\lambda_6\hat{v}^4) \tilde{h}_p + \sum_{\alpha} \tilde{g}_{-p}^{\alpha} (\hat{p}^2 + m_0^2 + 4\lambda\hat{v}^2 + 6\lambda_6\hat{v}^4) \tilde{g}_p^{\alpha} \right). \quad (11)$$

In this approach the bosonic determinant can no longer be neglected for in potential calculation, since it depends explicitly on the zero mode. Further, at first order in λ and λ_6 of perturbation theory, the propagator sums and combinatorial factors change,

$$\begin{aligned} U_2(\hat{v}) &= U_f(\hat{v}) + \frac{m_0^2}{2} \hat{v}^2 + \lambda \hat{v}^4 + \lambda_6 \hat{v}^6 \\ &+ \frac{1}{2V} \sum_{p \neq 0} \log \left[(\hat{p}^2 + m_0^2 + 12\lambda\hat{v}^2 + 30\lambda_6\hat{v}^4) \cdot (\hat{p}^2 + m_0^2 + 4\lambda\hat{v}^2 + 6\lambda_6\hat{v}^4)^3 \right] \\ &+ \lambda \left(3 \tilde{P}_H^2 + 6 \tilde{P}_H \tilde{P}_G + 15 \tilde{P}_G^2 \right) + \lambda_6 \hat{v}^2 \left(45 \tilde{P}_H^2 + 54 \tilde{P}_H \tilde{P}_G + 45 \tilde{P}_G^2 \right) \\ &+ \lambda_6 \left(15 \tilde{P}_H^3 + 27 \tilde{P}_H^2 \tilde{P}_G + 45 \tilde{P}_H \tilde{P}_G^2 + 105 \tilde{P}_G^3 \right), \end{aligned} \quad (12)$$

with the propagator sums given by:

$$\tilde{P}_H = \frac{1}{V} \sum_{p \neq 0} \frac{1}{\hat{p}^2 + m_0^2 + 12\hat{v}^2\lambda + 30\hat{v}^4\lambda_6}, \quad \tilde{P}_G = \frac{1}{V} \sum_{p \neq 0} \frac{1}{\hat{p}^2 + m_0^2 + 4\hat{v}^2\lambda + 6\hat{v}^4\lambda_6}. \quad (13)$$

In this approach logarithmic terms appear. Depending on the choice of the bare parameters ($m_0^2, \lambda, \lambda_6$), the arguments of the logarithms may become negative, leading to the well known problem that the effective potential becomes complex [25]. We remind, that the lattice spacing is set to one implicitly such that, even though we use the continuum notation, all quantities are dimensionless.

Using the analytical form of the CEP, the vev can be obtained by the (absolute) minimum of the potential. In order to introduce a physical scale, we set the lattice vev to the phenomenologically known value of 246 GeV and define the cutoff, Λ as the inverse lattice spacing:

$$\left. \frac{dU(\hat{v})}{d\hat{v}} \right|_{\hat{v}=vev} \stackrel{!}{=} 0, \quad \Lambda = \frac{246 \text{ GeV}}{vev}. \quad (14)$$

Further, the squared Higgs boson mass m_H^2 is determined by the second derivative of the potential at its minimum,

$$\left. \frac{d^2 U(\hat{v})}{d\hat{v}^2} \right|_{\hat{v}=vev} = m_H^2. \quad (15)$$

Due to the explicit appearance of the Higgs boson mass in the propagator sum eq. (7) for the potential U_1 , eq. (8), we have to use an iterative approach in the determination of a solution for the minimum of the CEP and the Higgs boson mass. To this end, we fix the parameters m_0^2 , y , λ and λ_6 , guess an initial Higgs boson mass and simply iterate eqs. (14,15) until we find convergence.

We will compare results obtained from both forms of the potential to results from our non-perturbative simulations. As we will see below, we indeed find parameter sets, where the perturbative CEP describes the non-perturbative data well, even on a quantitative level. This will allow us to obtain results for the phase structure of the Higgs-Yukawa model considered here from the analytical perturbative CEP, where a non-perturbative simulation is not feasible anymore, i.e. for large lattices or large cut-offs.

4. Results

For our study of the phase structure we performed simulations for two values of λ_6 (0.001 and 0.1). Note, that having set the lattice spacing to one, λ_6 is treated as a dimensionless coupling constant. For each value of λ_6 we choose a set of values for the quartic coupling, λ . The Yukawa coupling, y , is chosen such that the quarks in our model have a mass of that of the physical top quark, $m_t = y \cdot vev \cdot \Lambda \approx 175$ GeV. The phase transition between the symmetric and spontaneously broken phases is probed by scanning in the hopping parameter, κ .

In figure 1 we show results for the bare vev computed on lattices with volume $16^3 \times 32$ for $\lambda_6 = 0.001$ (left) and $\lambda_6 = 0.1$ (right). Our data show the same qualitative behaviour for both values of λ_6 . The phase transition is of second order when λ is chosen negative and its absolute value is small. Increasing the absolute value of λ will finally result in a change to a first order phase transition. The appearance of these first order phase transitions is a natural consequence of adding the dimension-6 operator, $(\varphi^\dagger \varphi)^3$, which can lead to multiple minima of the potential with non-vanishing vev .

For $\lambda_6 = 0.001$ which is shown in fig. 1a, the simulation data and the analytical results from both versions of the effective potential agree quite well. The results from U_2 , eq. (12), actually coincide with the simulation data on a quantitative level as long as the transition is of second order. The effective potential U_1 reproduces the behaviour of the simulation data qualitatively. However, the exact numerical results for the vev differ and the phase transitions are shifted to larger absolute values of λ .

For $\lambda_6 = 0.1$ which is shown in fig. 1b, the effective potential U_1 shows qualitative agreement with the simulations. The effective potential U_2 fails to describe the numerical data and the 1-loop evaluation of the CEP seems not to be sufficient.

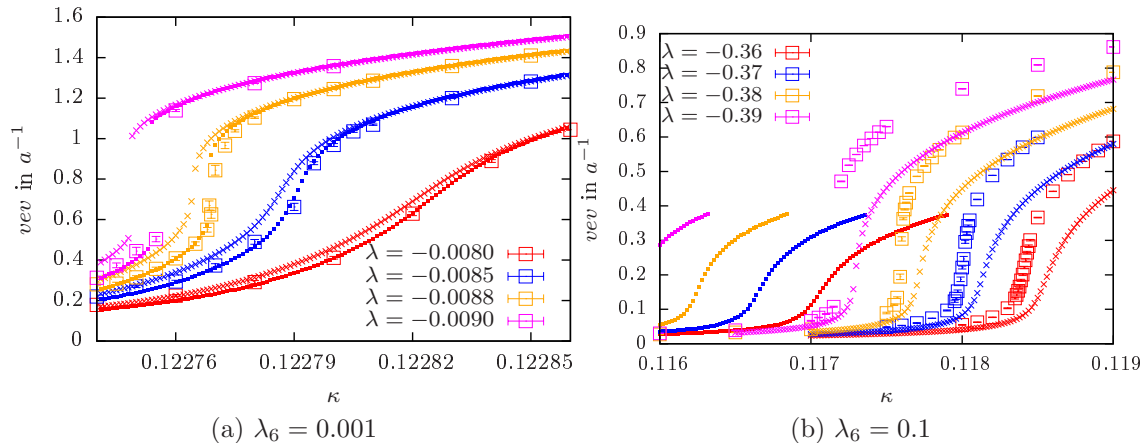


Figure 1: Data which were obtained from numerical simulations and the perturbative approaches described in section 3 are compared. The plots show the vev as a function of κ while λ_6 is kept fixed to $\lambda_6 = 0.001$ (left) and $\lambda_6 = 0.1$ (right) for various λ . The simulation data are depicted by the open squares, the crosses indicate the vev obtained from U_1 , eq. (8), while the dots show the corresponding results from U_2 , eq. (12). All data have been obtained on $16^3 \times 32$ lattices.

The results discussed above are obtained on a relatively small lattice of size $16^3 \times 32$. To verify the order of the phase transitions, simulations and analytical calculations on significantly larger lattices are necessary. In figure 2, we show results for the vev as a function of κ on various volumes. The parameters are chosen in a region where the small volume data indicate a second order transition, fig. 2a, and a first order transition, fig. 2b. In addition, we compare the simulation data to the analytical results from eq. (8) and eq. (12).

As it is shown in fig. 2a, the larger volume data confirm the second order nature of the phase transition. Furthermore, the finite volume dependence of the second order transition is very well described by both versions of the effective potential.

In fig. 2b, we show the vev obtained from the effective potential U_2 and from our non-perturbative lattice simulations on various volumes. Both methods give compatible results on a qualitative level and just the exact position of the phase transition is slightly altered. The jump in the vev indicates strongly the existence of a first order phase transition at a $\kappa_{\text{trans}} \approx 0.12277$. For these parameter choices, finite size effects are very small. In particular, for $\kappa \lesssim \kappa_{\text{trans}}$ the vev stays non-zero. This means that the first order transition occurs between two minima of the potential with non-zero vev . Hence, this transition must occur between two broken phases.

Close to the point where $\kappa \approx \kappa_{\text{trans}}$, tunneling events occur between the two minima in the simulations and hence the lattice simulation data may not agree with the results from the effective potential. This stems from the fact that the CEP gives only solutions at one of the minima and thus cannot take into account tunneling effects. In fig. 3a we show the Monte Carlo time history of \hat{v} at different values of κ which clearly shows tunneling events. While for $\kappa = 0.11757$ and $\kappa = 0.11763$ \hat{v} fluctuates around the mean value of $vev \approx 0.15$ and $vev \approx 0.40$, respectively, for

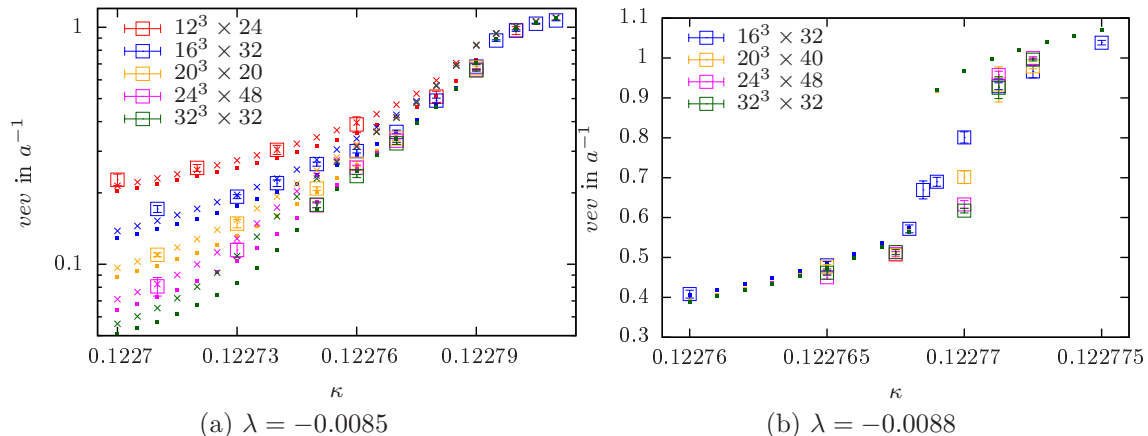


Figure 2: We show the finite volume effects of the phase structure scan for $\lambda_6 = 0.001$. The plot on the left hand side shows data for $\lambda = -0.0085$ where the simulations (open boxes) indicate a second order phase transition. The plot on the right hand side shows results for $\lambda = -0.0088$, where the transition is first order. In addition to the simulation data we show the data obtained from U_2 eq. (12) (dots) for both and from U_1 eq. (8) (crosses) for the left plot.

$\kappa = 0.11760$ tunneling events between these two values appear, typical for a first order phase transition.

From the histogram of \hat{v} with an appropriate binning size, we can construct an effective potential from the simulation data. This is shown in fig. 3b. It is demonstrated nicely how the absolute minimum at around $\hat{v} \approx 0.15$ abruptly jumps to $\hat{v} \approx 0.35$. Such a behaviour is typical for a first order transition.

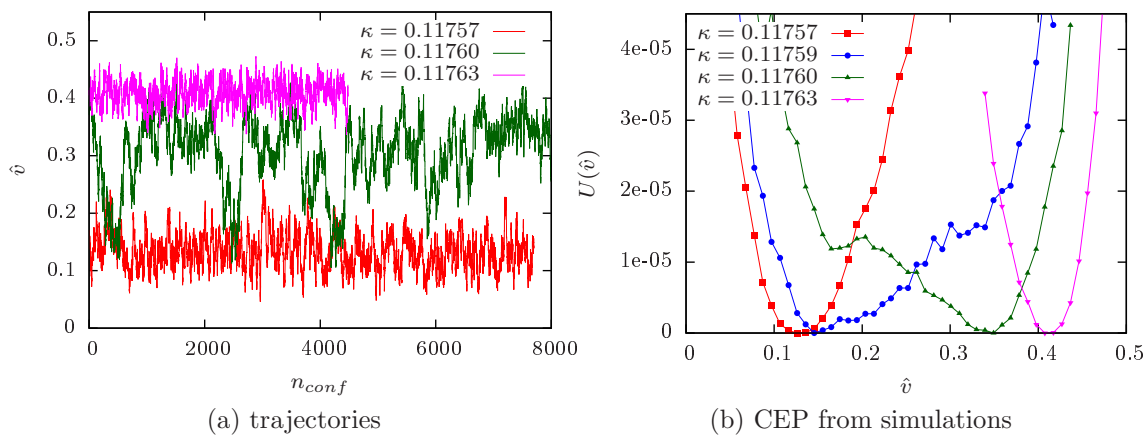


Figure 3: The left plot shows the trajectories for ensembles generated around the first order phase transition generated on 16×32 lattices. The data correspond to $\lambda_6 = 0.1$ and $\lambda = -0.38$. The right plot shows the corresponding CEP as it was obtained by taking the logarithm of the histograms of the magnetization. The lines in (b) just serve to guide the eye.

Given the fact that for small values of λ_6 the effective potentials describe the simulation data on a quantitative level, it can be utilized to investigate the behaviour of the vev further. Due to the wider range of applicability we restrict ourselves in

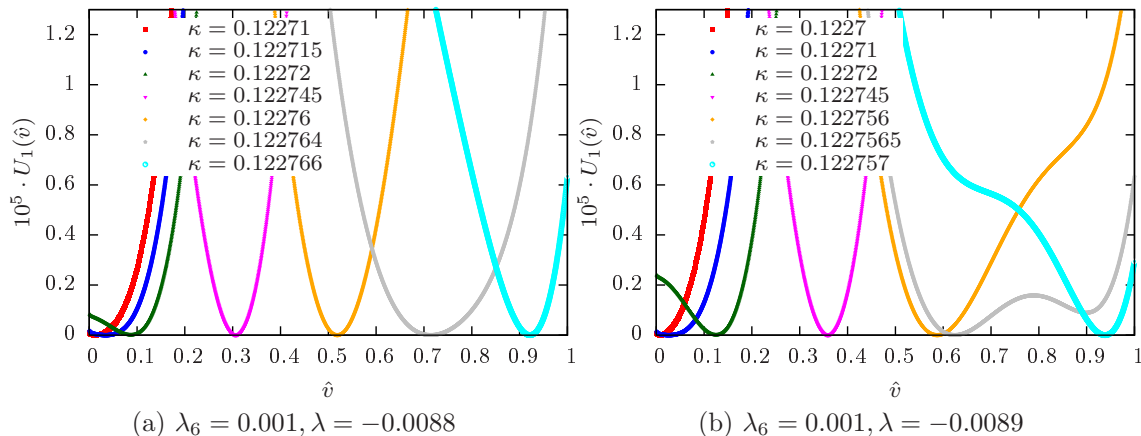


Figure 4: Here we show the CEP U_1 , eq. (8), for fixed $\lambda_6 = 0.001$ and various κ values around the phase transition. The left plot ($\lambda = -0.0088$) shows a second order phase transition for $\kappa \approx 0.122715$. Note that the effective potential at $\kappa \approx 0.122764$ actually corresponds to a crossover transition, see the discussion in the text and fig. 5. The right hand plot ($\lambda = -0.0089$) also shows a second order transition at $\kappa \approx 0.12271$ and a first order transition $\kappa \approx 0.1227565$

the following discussion to the potential U_1 , eq. (8).

We plot the behaviour of the effective potential as a function of κ in figure 4 for a fixed value of $\lambda_6 = 0.001$. In fig. 4a, the behaviour of the effective potential shows a second order phase transition: the minimum moves from a zero to a non-zero value in a smooth way, indicating the second order nature of the transition.

However, when λ is slightly changed to $\lambda = -0.0089$ we observe, in addition to a second order transition at $\kappa \approx 0.12271$, a phase transition from one non-zero value of the vev to another non-zero value of the vev at large κ -values, as shown in fig. 4b. This transition happens through a double well potential which is almost realized at $\kappa = 0.1227565$.

To determine the location of a second order transition in the CEP, we investigate the curvature of the potential at its minimum, $U''(vev)$. The curvature of the potential in its minimum is related to the susceptibility χ of the magnetization, $\chi \propto 1/U''(vev)$, and is therefore minimal at the location of the second order transition. The susceptibility at the phase transition diverges when the volume goes to infinity corresponding to $U''(vev)$ going to zero. To study this finite size effect, we investigate the behaviour of the vev and the inverse curvature of the potential for volumes up to $128^3 \times 256$. Some example plots are shown in fig. 5 where we plot $1/U''(vev)$ as a measure of the magnetic susceptibility. In fig. 5a the typical behaviour for a second order transition is apparent for $\lambda = -0.007$. For $\lambda = -0.0085$ (fig. 5b) a second maximum in the inverse curvature of the potential is visible. This second maximum is volume independent and indicates a crossover transition in the broken phase. In fig. 5c the second transition at $\kappa = 0.12275$ has turned into a first order one, while the second order transition between the symmetric and broken phase is still present at smaller values of κ .

Our results for the phase structure computed within the framework of the CEP

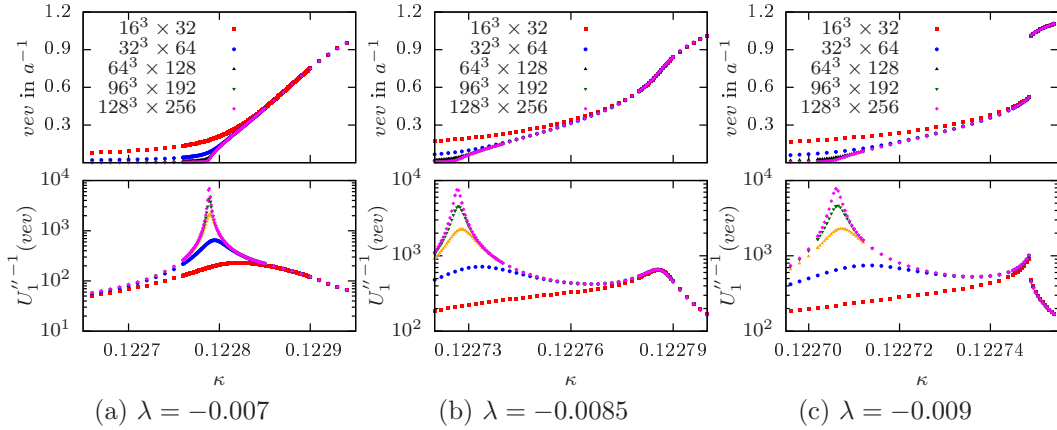


Figure 5: Here the volume dependence of the location of the minimum of the CEP U_1 , i.e. the vev (upper plots) and its inverse curvature in the minimum as a measurement for the magnetic susceptibility (lower plots) are shown as a function of κ for $\lambda_6 = 0.001$ and a set of λ -values.

are summarized in fig. 6 for both λ_6 values. For $\lambda_6 = 0.001$ we clearly observe a second order phase transition at small absolute values of λ . At intermediate absolute values of λ an additional crossover transition sets in within the broken phase. This crossover turns into a first order phase transition around $\lambda \approx -0.0089$. The second order transition still exists at this point separating the broken and symmetric phases. Around $\lambda \approx -0.0098$ and $\kappa \approx 0.12267$ the line of second order transition runs into the line of first order transition. From that point on only the first order transition remains separating the symmetric and broken phases.

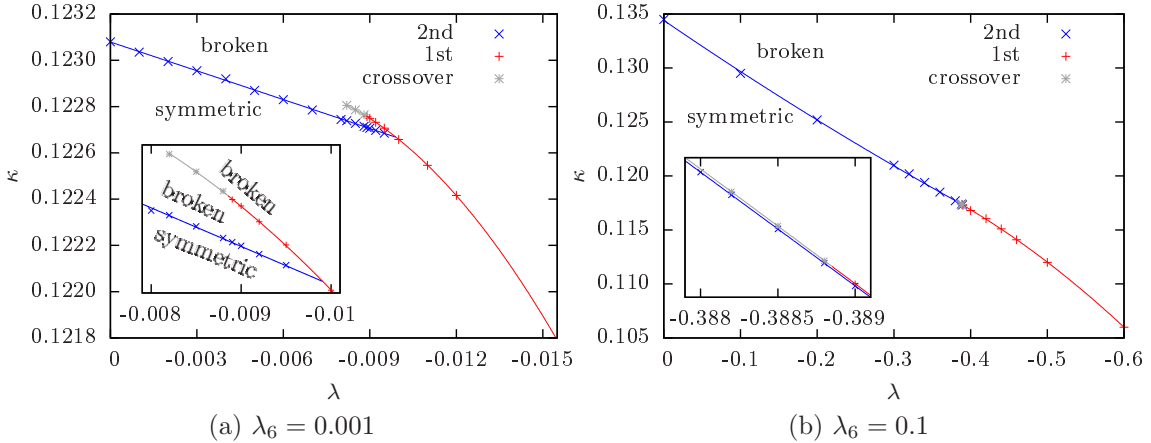


Figure 6: Phase structure obtained from the CEP U_1 (8). There are two phases - a broken and a symmetric one - separated by lines of first and second order phase transitions. Furthermore there is a small region in parameter space, where a first order transition between two broken phases exists for $\lambda_6 = 0.001$ and $\lambda_6 = 0.1$. The lines between the data points are just to guide the eye.

For $\lambda_6 = 0.1$ the general behaviour is very similar. However, the region in parameter space where the additional transitions between two broken phases occur

is extremely narrow, see the inlet in fig. 6b. In fact, the region is so narrow that it is well possible that in infinite volume only a single transition line exists with second order transitions for larger and first order transitions for smaller quartic couplings.

With the CEP the Higgs boson mass can also be obtained from eq. (15). In figure 7 we show some first results for the cut-off dependence of the Higgs boson mass obtained by the CEP U_1 for a series of λ values around the region where the first order transitions appear. For $\lambda_6 = 0.001$ we observe, see fig. 7a, that for the range of cut-off values considered here, the Higgs boson mass can be lowered compared to the lower Higgs boson mass for vanishing self couplings λ and λ_6 as was also found in ref. [1].

Inspecting, however, fig. 7b we find that for $\lambda_6 = 0.1$ and for small cut-off values, the Higgs boson mass is significantly larger than the lower bound at vanishing λ and λ_6 . Note that $m_H/\Lambda \approx 0.1$, i.e. we are still staying in the scaling region of the model. The increase of the Higgs boson mass at small cut-off can be understood from the fact that the $\lambda_6(\Phi^\dagger\Phi)^3$ term in the action provides a positive contribution to the Higgs boson mass shift, dominating the negative contribution from the Yukawa coupling. For larger values of the cut-off, the λ_6 coupling becomes less and less relevant and the Yukawa term provides the major contribution to the mass-shift such that we eventually find the standard behaviour of the Higgs boson mass as a function of the cut-off in fig. 7b.

We plan to investigate the cut-off dependence of the Higgs boson mass through non-perturbative numerical simulations in the future. However, if the picture of fig. 7b is confirmed, this would lead to a bound on the values of λ_6 since the 126 GeV Higgs boson mass would be in conflict with the cut-off dependent mass at low values of the cut-off. As a consequence, only rather small values of $\lambda_6 \propto O(0.001)$ would be compatible with the 126 GeV Higgs boson mass.

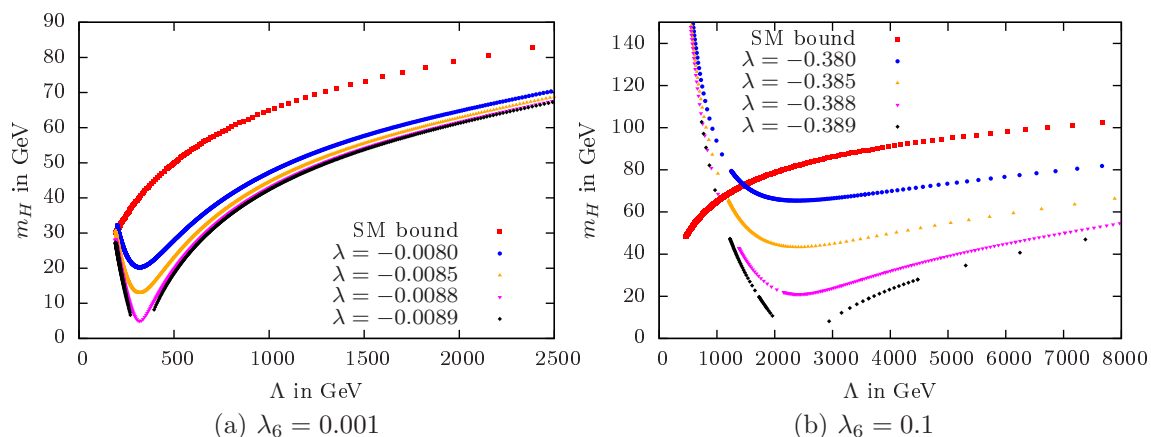


Figure 7: Shown is the cut-off dependence of the Higgs boson mass obtained from the CEP according to eq. (14) for $\lambda = 0.001$ on a $64^3 \times 128$ -lattice (left) and $\lambda = 0.1$ on a $192^3 \times 384$ (right). In both plots we also show the standard model lower mass bound ($\lambda_6 = \lambda = 0$).

5. Conclusions

In this letter we focused on the investigation of the phase structure of a chirally invariant lattice Higgs-Yukawa model including an additional higher dimensional operator, $(\varphi^\dagger\varphi)^3$, with coupling strength λ_6 in the action. For the analysis of such a system we restricted ourselves to small values of λ_6 for now. This allowed us to compare our numerically obtained results with analytical predictions from the constraint effective potential evaluated in the same lattice setup as the numerical simulations were carried through.

In general, we obtained a very good qualitative and even quantitative agreement between both approaches leading to the phase structure shown in fig. 6 for fixed values of $\lambda_6 = 0.001$ and $\lambda_6 = 0.1$.

Fixing $\lambda_6 > 0$ stabilizes the potential, allowing thus to drive the values of λ more and more negative. For sufficiently small values of λ we observe smooth transitions in the magnetization, fully compatible with the second order phase transitions observed for $\lambda_6 = 0$. However, from a certain negative value of λ on, we find an additional phase transition which can be a crossover or first order transition. Indications for these transitions can be detected from the behaviour of the magnetization computed both in the effective potential and the numerical simulations, see e.g. fig. 4b. Thus, the resulting phase diagram in fig. 6 turned out to be rather rich with second and first order phase transition lines when changing κ . We note in passing that by fixing the hopping parameter κ and hence the bare Higgs boson mass, it is possible, to move to a broken phase by only changing the quartic coupling of the theory.

A natural extension of the investigation here would be the exploration of the phase structure of the model at non-zero temperature. Our results show that a simple extension of the Higgs-Yukawa sector of the standard model by a $(\phi^\dagger\phi)^3$ term leads to first order phase transitions. This might open the possibility to generate a strong enough first order phase transition at a non-zero temperature which is compatible with baryogenesis [26] even at a value of the Higgs boson mass of 126 GeV.

The constraint effective potential also allows to compute the Higgs boson mass from the second derivative at its minimum. By fixing the value of $\lambda_6 = 0.001$ and driving λ more and more negative, we obtain lower and lower values of the Higgs boson mass and, in particular, substantially smaller values than obtained for $\lambda_6 = 0$ at a comparable value of the cut-off. This finding is fully compatible with the results of [1]. As a criterion to obtain an absolute lower bound for the Higgs boson mass one may choose the value of the quartic coupling, where the second order standard model like phase transition turns into a first order one since in the Higgs-Yukawa sector of the SM itself only second order phase transitions occur.

We have also found that for larger values of $\lambda_6 = 0.1$ and at small values of the cut-off the positive contribution of the λ_6 term to the Higgs boson mass-shift leads to significantly enhanced Higgs boson masses. In fact, we can already exclude certain values of the quartic and λ_6 couplings since there the 126 GeV Higgs boson mass is in conflict with the lower bounds obtained here. It will be interesting to perform a

more systematic study of the lower Higgs boson mass bounds at additional values of λ_6 . By employing also numerical simulations this can provide exclusion bounds for the coupling values and hence for models which lead to an extension of the standard model with a $(\phi^\dagger\phi)^3$ term. We plan to carry out such investigations in the future.

Acknowledgments

We thank K. Nagai for ongoing discussions and M. Müller-Preussker for his continuous support. We moreover acknowledge the support of the DFG through the DFG-project *Mu932/4-4*, the support from Taiwanese MOST via grant *102-2112-M-009-002-MY3* and the support from the DAAD-MOST exchange programme via *project 57054177*. The numerical computations have been performed at the DESY Zeuthen computer center and on the *SGI system HLRN-II* at the HLRN Supercomputing Service Berlin-Hannover.

References

- [1] Holger Gies, Clemens Gneiting, and René Sondenheimer. Higgs Mass Bounds from Renormalization Flow for a simple Yukawa model. Phys.Rev., D89:045012, 2014.
- [2] Holger Gies and René Sondenheimer. Higgs Mass Bounds from Renormalization Flow for a Higgs-top-bottom model. 2014.
- [3] John Ellis, Veronica Sanz, and Tevong You. Complete Higgs Sector Constraints on Dimension-6 Operators. JHEP, 1407:036, 2014.
- [4] Anke Biekötter, Alexander Knochel, Michael Kraemer, Da Liu, and Francesco Riva. Vices and Virtues of Higgs EFTs at Large Energy. 2014.
- [5] Vincenzo Branchina and Emanuele Messina. Stability, Higgs Boson Mass and New Physics. Phys.Rev.Lett., 111:241801, 2013.
- [6] Vincenzo Branchina, Emanuele Messina, and Alessia Platania. Top mass determination, Higgs inflation, and vacuum stability. JHEP, 1409:182, 2014.
- [7] Astrid Eichhorn, Holger Gies, Joerg Jaeckel, Tilman Plehn, Michael M. Scherer, et al. The Higgs Mass and the Scale of New Physics. 2015.
- [8] Martin Lüscher. Exact chiral symmetry on the lattice and the Ginsparg-Wilson relation. Phys.Lett., B428:342–345, 1998.
- [9] Paul H. Ginsparg and Kenneth G. Wilson. A Remnant of Chiral Symmetry on the Lattice. Phys.Rev., D25:2649, 1982.
- [10] Herbert Neuberger. Exactly massless quarks on the lattice. Phys.Lett., B417:141–144, 1998.

- [11] Herbert Neuberger. More about exactly massless quarks on the lattice. Phys.Lett., B427:353–355, 1998.
- [12] Pilar Hernandez, Karl Jansen, and Martin Lüscher. Locality properties of Neuberger’s lattice Dirac operator. Nucl.Phys., B552:363–378, 1999.
- [13] P. Gerhold and K. Jansen. The Phase structure of a chirally invariant lattice Higgs-Yukawa model for small and for large values of the Yukawa coupling constant. JHEP, 0709:041, 2007.
- [14] P. Gerhold and K. Jansen. The Phase structure of a chirally invariant lattice Higgs-Yukawa model - numerical simulations. JHEP, 0710:001, 2007.
- [15] P. Gerhold and K. Jansen. Lower Higgs boson mass bounds from a chirally invariant lattice Higgs-Yukawa model with overlap fermions. JHEP, 0907:025, 2009.
- [16] P. Gerhold and K. Jansen. Upper Higgs boson mass bounds from a chirally invariant lattice Higgs-Yukawa model. JHEP, 1004:094, 2010.
- [17] P. Gerhold, K. Jansen, and J. Kallarackal. Higgs boson mass bounds in the presence of a very heavy fourth quark generation. JHEP, 1101:143, 2011.
- [18] J. Bulava, K. Jansen, and A. Nagy. Constraining a fourth generation of quarks: non-perturbative Higgs boson mass bounds. Phys.Lett., B723:95–99, 2013.
- [19] Philipp Gerhold, Karl Jansen, and Jim Kallarackal. The Higgs boson resonance width from a chiral Higgs-Yukawa model on the lattice. Phys.Lett., B710:697–702, 2012.
- [20] John Bulava, Philipp Gerhold, Karl Jansen, Jim Kallarackal, Bastian Knippschild, et al. Higgs-Yukawa model in chirally-invariant lattice field theory. Adv.High Energy Phys., 2013:875612, 2013.
- [21] L. O’Raifeartaigh, A. Wipf, and H. Yoneyama. The Constraint Effective Potential. Nucl.Phys., B271:653, 1986.
- [22] Roberto Frezzotti and Karl Jansen. The PHMC algorithm for simulations of dynamical fermions: 1. Description and properties. Nucl.Phys., B555:395–431, 1999.
- [23] P. Gerhold. Upper and lower Higgs boson mass bounds from a chirally invariant lattice Higgs-Yukawa model.
- [24] R. Fukuda and E. Kyriakopoulos. Derivation of the Effective Potential. Nucl.Phys., B85:354, 1975.
- [25] Erick J. Weinberg and Ai-qun Wu. UNDERSTANDING COMPLEX PERTURBATIVE EFFECTIVE POTENTIALS. Phys.Rev., D36:2474, 1987.

- [26] Andrew G. Cohen, D.B. Kaplan, and A.E. Nelson. Progress in electroweak baryogenesis. Ann.Rev.Nucl.Part.Sci., 43:27–70, 1993.